Chapter 6
Electrochemical Synthesis of Dispersed Metallic Nanoparticles

Luca Magagnin and Paula Cojocaru

6.1 Introduction

Micro- and nanosized particles of noble and precious metals, with size uniformity, morphological homogeneity, and high purity, are a class of material of great interest for many applications in the field of nanotechnology, due to their unusual catalytic and physical–chemical properties, and for their possible exploitation in catalysis and advanced technology applications. Several techniques have been employed aiming at the fabrication of nanoparticles of different metals, e.g. the chemical reduction of the chloro-metallate anion, metal vapor synthesis, and electrochemical deposition [1–8]. Some other methods are being used for the preparation of gold nanoparticles like sol–gel, deposition–precipitation, and dip-coating techniques [9, 10]. Of these, recent studies have shown that electrodeposition is an easy and a fast procedure for the preparation of nanoparticles on a substrate [6, 11].

Electrochemical synthesis of metal powder has been traditionally used for mass production of micrometer size powder being primarily used in powder metallurgy as well as other engineering applications [12].

L. Magagnin (✉) • P. Cojocaru
Dip. Chimica, Materiali e Ing., Chimica G. Natta, Politecnico di Milano, Via Mancinelli, 7, 20131 Milano, Italy
e-mail: luca.magagnin@polimi.it; paula.cojocaru@polimi.it

Stojan S. Djokić (ed.), *Electrochemical Production of Metal Powders*, Modern Aspects of Electrochemistry 54, DOI 10.1007/978-1-4614-2380-5_6,

The electrochemical synthesis of metal nanoparticles and other nanostructures is being currently considered as a potential route for the development of advanced functional materials and devices in different technology area, including chemical sensing, magnetic storage, microelectronics, electroanalysis, and electrocatalysis [13–17].

6.2 Electrolytic Synthesis of Nanoparticles

Two major parameters control the chemical, physical, and electrocatalytic properties of the nanoparticles, namely, the particle size and shape (and the crystallographic orientation) of the nanometer scale material. The control of the size and geometry of the prepared nanoparticles remains a difficult aspect. To decrease dispersion in particle size during electrocrystallization, two important principles should be taken into account. First, the crystal seed formation should occur instantaneously thus preventing progressive nucleation. Second, the crystal growth has to be conducted at a slow rate, i.e., at low overvoltage. The importance and coherence of these fundamental principles has been recently elucidated by Penner et al. [18–22]. His research group successfully started extensive investigations on the electrodeposition of silver, gold, platinum, and cadmium nanoparticles on graphite surfaces [18–22]. The ideal method for transforming both principles which favor monodispersity into an experimental procedure can be best attained by applying the potentiostatic double-pulse technique. This method introduced by Scheludko and Todorova is based on an extremely short nucleation pulse of high cathodic polarization followed by a much longer growth pulse at low cathodic overvoltage [23, 24]. The ideal model situation is where nucleation only occurs within the first pulse and exclusive particle growth during the second pulse. The first pulse is more negative than E_{CRIT}, the critical potential for nucleation, and the second pulse is more positive than E_{CRIT} but more negative than the reversible potential (Fig. 6.1). The high cathodic amplitude of the first pulse is necessary to initiate nucleation. To achieve this, the overpotential of the second pulse must be low enough to inhibit generation of new nuclei. Under such circumstances, the original

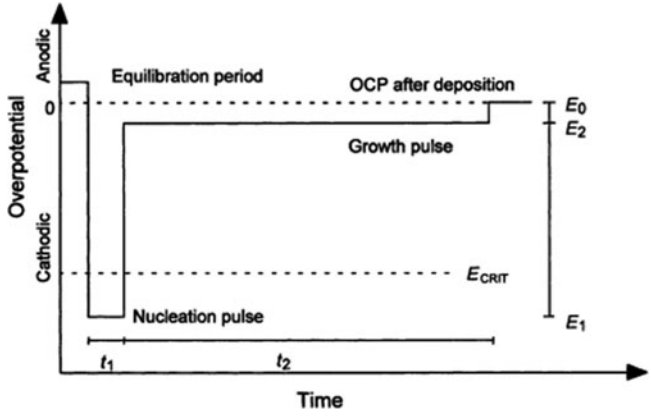

Fig. 6.1 Schematic representation of the potentiostatic double-pulse method. After an equilibration period, a nucleation pulse of potential E_1 is applied for a time t_1. To form nucleation sites, E_1 must be more negative than the critical nucleation potential E_{CRIT}. The first pulse is immediately followed by a growth pulse of potential E_2 for a time t_2. As E_2 is more positive than E_{CRIT}, no further nucleation on the substrate is possible (Reprinted from [24], Copyright 2002 with permission from Elsevier Science [24].)

distribution of stable nuclei formed during the first pulse should be preserved. With this method, the conflict between both optimal conditions for nucleation and growth is partially defused. This is due to the amount of small seed additionally nucleated at the higher polarization and resolved as soon as the potential is switched over to the lower polarization of the growth pulse. According to theory, the double-pulse procedure is an efficient way to control the particle size distribution of depositions.

Very recently, pulsed sonoelectrochemical synthesis, which was first introduced by Reisse et al. and involves alternating sonic and electric pulses, has been employed to obtain shape-controlled synthesis of nanoparticles [25–28]. The present understanding of the sonoelectrochemical mechanism describes an electrochemical deposition of a thin layer on the sonoelectrode during the electric pulse. The thin layer is then destroyed by the coming sonic pulse, to form jet-suspended nanoparticles in the solution. The electrochemical and sonic parameters, including the pulse duration, can be used to control

the particle characteristics. For example, Gedanken et al. have reported the use of pulse sonoelectrochemistry for the preparation of silver nanoparticles with different shapes, including spherical, rodlike, and dendritic nanoparticles, and uncovered the crucial role of electrolyte composition in the shape formation [29]. According to their explanation, during sonication the particles are not completely detached from the sonoelectrode, so that the particles formed in the next pulse can further grow on seeds that are left on the surface.

To control the size and geometry of the prepared nanoparticles, another important parameter is the kind of substrate used. According to Markov et al. when metal crystallites or drops nucleate or grow onto a foreign substrate, in their immediate vicinity zones of zero nucleation probability exist [30]. Nucleation under these conditions occurs under the influence of the external electrical field. The growth of nuclei causes deformations in the field, resulting in an overpotential drop in the screened surface segments. When the overpotential is lower than the minimum value for nucleation, further nucleation is impossible. It was shown that for a hemispherical drop on a flat substrate, nucleation is impossible inside a zone of radius r, defined as

$$r = f\frac{E}{E - E_k}\rho, \tag{6.1}$$

where f is a numerical factor accounting for the deviation of geometry, E is cell voltage, and E_k is the critical voltage for nucleation. When $E > E_k$, the zone radius, r, approaches the effective value of the drop size. This explanation is valid only for processes under ohmic control, for example, for deposition of metals having high exchange current densities, as is the case with silver [31, 32]. Another possibility is the deposition of a metal onto its own surface as substrate. In this case, nucleation is also a prerequisite for the deposition process to start, but the critical overpotential value, E_k, is much lower than on a foreign substrate.

Recently, electrodeposition has been proved to provide a versatile method for producing metal nanoparticles and nanowires in the pores of polycarbonate, mica, and aluminum oxide templates [33–36]. In this case, the template imparts size control. Behm et al. obtained

periodic arrays of size-similar metal islands by electrochemically decorating defects on the reconstructed gold (111) surface [37–39]. Kolb et al. transferred electrodeposited metal from the tip of an atomic force microscope to a metal surface [40–42]. Metal nanoparticles narrowly dispersed in size were thereby obtained. For example, hundreds of copper nanoparticles were positioned in a square array on a gold surface using this approach. The small size of these particles makes them ideal catalysts for many chemical as well as electrochemical applications [10, 11, 43]. For instance, Au nanoparticles were found to have extraordinary electrocatalytic properties towards the electrochemical reduction of molecular oxygen in acidic media, for the catalytic hydrogenation of unsaturated alcohols and aldehydes, as well as for the low-temperature oxidation of carbon monoxide [10, 11, 43]. Several other applications of Au nanoparticles are currently emerging to include reduction of NO with propene, CO, or H_2, removal of CO from H_2 streams, selective oxidation, e.g., epoxidation of olefins, as well as a selective hydrogenation of CO and CO_2 [44]. Additionally, recent studies have shown that these nanometer scale materials can be used to form quantum dots.

6.3 Sonoelectrochemical Synthesis of Nanoparticles

Sonoelectrochemistry is concerned with the coupling of power ultrasound to electrochemical systems to achieve and develop new processes [45, 46]. Ultrasounds are known to cause a multitude of complex phenomena such as turbulent flow, bubble oscillation and cavitation, generation of microjets, and shock waves [47, 48]. So far, many reports with empirical findings, predominantly the massive increase in the rate of mass transport at the electrode–solution interface, have appeared. Most experimental findings confirm that ultrasound effects are mainly related to mass transport and thermal effects. The mass transport model has been developed into some detail and it is now possible to qualitatively predict the mass transport parameters for certain cell designs and/or ultrasound sources depending on the effect of acoustic streaming [49].

The application of ultrasound irradiation to electrochemistry processes dates back to the 1930s [50]. However, in the last decade the expansion of the sonoelectrochemistry has become increasingly important. Since recently there is a growing interest of the application of the sonoelectrochemistry in environmental remediation and in the preparation of nanopowders. Reisse et al. have described a device for the production of metal powders using pulsed sonoelectrochemical reduction [51]. In those experiments a titanium probe (20 kHz) acts both as a cathode and as an ultrasound emitter [51, 52]. The electroactive part of the sonoelectrode is the planar circular surface at the bottom of the horn and the immersed cylindrical part into the electrolyte is covered by an isolating plastic jacket. The ultrasound probe is connected to a generator and a potentiostat using a pulse driver. The use of a three-electrode configuration (working, reference, and auxiliary electrodes) rather than just a cathode and an anode in a sonoelectrochemistry system was later proposed to apply a controlled potential to the sonoelectrode to get a better control of the process. In the majority of cases the processes have been carried out under galvanostatic conditions. Pulsed sonoelectrochemistry techniques, which use 20 kHz ultrasound horn both as a working electrode and as an ultrasound emitter, have been used to prepare nanopowders. The majority of nanomaterials produced by this method are pure metals. More recently the syntheses have been extended to include the preparation of nanosized metallic alloys, metal oxide semiconductors, and conductive polymers. The ultrasound pulse time and the current density are fundamental for controlling the process yield and particle size: a decrease in size can be achieved by decreasing the temperature, shortening the pulse duration, and increasing the current density and the ultrasound intensity. Nanoparticles aggregates can be formed, even if the shape and size of the nanoparticles can be tailored through the operational parameters and using suitable stabilizers [53].

The present importance of sonoelectrochemistry emerges from the wide range of its applications [54]. The first documented application of an ultrasound field was focused on electroplating. Nowadays, different nanomaterials are prepared by sonoelectrochemical methods. Nanoparticles of magnesium, tungsten, copper, palladium, silver, gold, PbS, copper oxide (I), Au–Ag alloys, and Co–Fe alloys have been synthesized by sonoelectrochemistry. In the same way, nanotubes of CdSe and TiO_2 and silver nanowires have also been synthetized [54–60].

6.4 Experimental Considerations for Electrolytic Synthesis of Nanoparticles

The development and the characterization of an electrochemical process for the synthesis of silver and gold particles from sulfite-based electrolytes are discussed in this section. The solution chemistry is selected in alternative to electrolyte composition inherited from chemical deposition processes and on the basis of its environmental benignity and reasonable chemical stability. The electrolyte composition was preliminary tested and, if needed, modified by adding appropriate components. The electrochemical deposition of silver nanoparticles was carried out from an electrolyte of the following base composition: $AgNO_3$ in the range from 10^{-3} to 0.1 M; $NaNO_3$ in the range from 0.05 to 0.5 M; Na_2SO_3 0.25 M, at pH 8.6. By slowly adding dilute silver nitrate solution to a stirred solution of sodium sulfite and sodium nitrate, precipitation of Ag_2S was avoided. Gold nanoparticles were electrodeposited from an electrolyte containing gold ammonium sulfite $(NH_4)_3Au(SO_3)_2$ 10 mM, Na_2SO_3 0.1 M, and ethylenediamine $C_2H_8N_2$ 10 mM, at pH 6.5. All solutions were prepared using reagent grade chemicals and double distilled water. Deposition tests were performed at room temperature (Ag) or at 55°C (Au). Electrochemical experiments were carried out in a conventional three electrode cell using as working electrode either an amorphous glassy carbon GC disc, apparent surface area 0.2826 cm^2, a titanium sheet or an indium–tin oxide (ITO) substrate, on which an apparent surface area of 1 cm^2 was defined by an insulating tape. The amorphous carbon electrode was polished by 1 μm diamond paste, ultrasonically washed in alcohol and distilled water and finally dried in a nitrogen stream. The titanium sheets were etched in dilute HF solution and polished with 1200 grit paper, ultrasonically washed in distilled water and air dried. A saturated calomel electrode (SCE) served as a reference electrode. The counter electrode was a platinum wire with a much larger surface area than the working electrode. The electrochemical characterization of metal particles deposition was carried out by cyclic voltammetry using a model 273A EG&G PAR potentiostat. The scan rate during voltammetric cycling was changed in the range from 50 to 300 mV s^{-1}. The formation of particles and their morphological

features, characterized by scanning electron microscopy, was examined focusing on deposition on titanium substrate, in view of the possible exploitation of nanoparticles deposition as a method to modify and functionalize an electrodic material of widespread industrial use.

6.5 Deposition of Silver Nanoparticles

Cyclic voltammetry was first employed to define the potential region of the deposition process at changing Ag(I) concentration. The electrode potential was driven in the cathodic direction from 0.7 to −0.7 V at a scan rate of 100 mV s^{-1}. Figure 6.2 shows typical voltammetric curves at the glassy carbon electrode changing Ag(I) concentration in solution from 1 to 30 mM.

The peak potential for the cathodic reduction of the silver sulfite complex $[Ag(SO_3)_2]^{3-}$ shifts towards more positive value as the

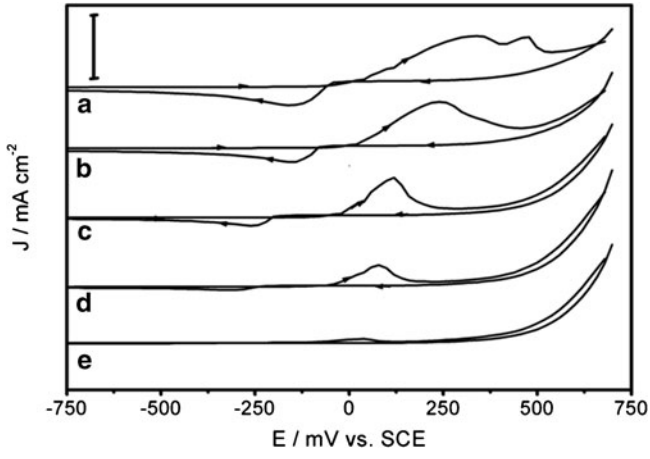

Fig. 6.2 Cyclic voltammograms from 0.7 to −0.7 V at glassy carbon electrode in electrolyte with changing Ag(I) concentration, Na_2SO_3 0.25 M, $NaNO_3$ 0.1 M, at pH 8.6; Ag(I): (**a**) 3×10^{-2} M, (**b**) 2×10^{-2} M, (**c**) 1×10^{-2} M, (**d**) 5×10^{-3} M, (**e**) 1×10^{-3} M. Scale bar 1 mA cm^{-2}

Ag(I) concentration increases, indicating the lowering of the nucleation overpotential as the silver concentration is increased. The formal potential of the complex may be estimated as about 0.02 V SCE by using the reported value of the stability constant ($\log K \approx 9.0$) [61]. This is qualitatively confirmed by the voltammetric analysis, observing that, as the Ag(I) concentration increases, the potential value midway between the anodic and cathodic peaks approaches the value of the formal potential as given above. In each voltammogram, two distinct current peaks are clearly resolved. The first peak, which is distinctly seen for Ag(I) concentration in excess of 5 mM, is associated with the Ag(I) reduction process whereas the second peak represents the Ag dissolution process from the amorphous carbon substrate. For Ag(I) concentration 1 mM the voltammogram presents only a shallow wave during the cathodic semicycle, and no crossing of forward and reverse scan is observed, suggesting that nucleation is very limited in these conditions. The peak parameters, current density, and potential change significantly as the Ag(I) concentration increases: the potential of both peaks shift towards more positive values, as expected; besides, both peaks change in shape, showing broadening, and the crossing of the forward and reverse scan becomes more and more evident, as a result of increased nucleation intensity. The anodic current peak suddenly appearing in the voltammogram at Ag(I) concentration 0.03 M may be attributed to the oxidation of dithionite [62].

The above mentioned changes occurring in the silver deposition process at increasing Ag(I) concentration were further characterized. As shown in Fig. 6.3 in the case of Ag(I) 20 mM solution, a linear relationship between the peak current and the root square of the potential scan rate $v^{1/2}$ was found in the range 50–300 mV s^{-1}. In addition, as shown in Fig. 6.4, a linear relationship is found between the peak current density at a fixed potential scan rate and the concentration of Ag(I). These observations indicate that the cathodic reduction of the electroactive species is controlled by diffusive transport [63]. The relationship determined between peak current density and the Ag(I) concentration, as shown by the graph in Fig. 6.4, supports this conclusion.

A further step in this work was to test the effect of a supporting electrolyte on the electrodeposition of silver particles. To this aim,

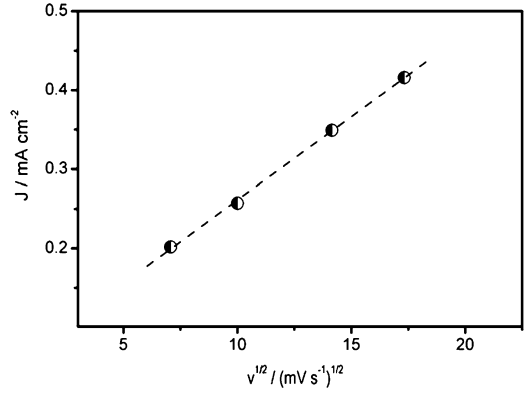

Fig. 6.3 Change of peak current density with potential scan rate at the glassy carbon electrode in Na_2SO_3 0.25 M, $NaNO_3$ 0.1 M, and Ag(I) 20 mM, at pH 8.6

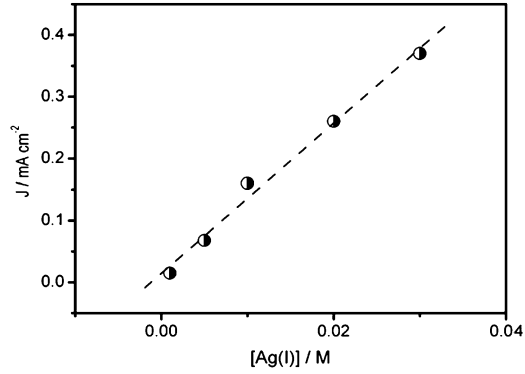

Fig. 6.4 Peak current density at scan rate 100 mV s^{-1} vs. Ag(I) concentration

sodium nitrate $NaNO_3$ was added in increasing concentration to the silver sulfite electrolyte and a cyclic voltammetry characterization (Fig. 6.5) at the glassy carbon electrode was performed. The current density and the potential of voltammetric peaks changed significantly as the sodium nitrate concentration was varied in the deposition bath. In Fig. 6.6 the trend of cathodic peak current density versus $NaNO_3$

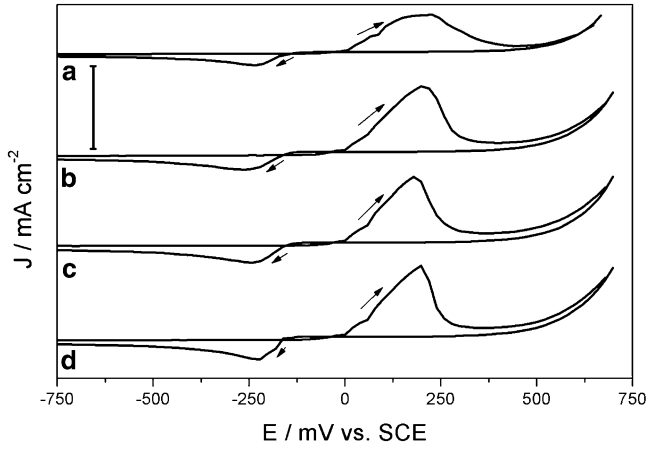

Fig. 6.5 Cyclic voltammograms from 0.7 to −0.7 V at glassy carbon electrode in electrolyte with changing $NaNO_3$ concentration, Na_2SO_3 0.25 M, Ag(I) 20 mM, at pH 8.6; $NaNO_3$ conc.: (**a**) 4×10^{-1} M, (**b**) 3×10^{-1} M, (**c**) 2×10^{-1} M, (**d**) 5×10^{-2} M. Scale bar 1 mA cm^{-2}

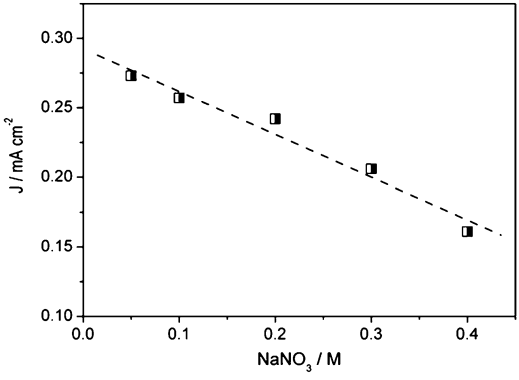

Fig. 6.6 Cathodic peak current density from cycling voltammograms (100 mV s^{-1}) at glassy carbon electrode versus $NaNO_3$ concentration. The electrolyte composition is the following: Ag(I) 20 mM, Na_2SO_3 0.25 M, $NaNO_3$ as reported, pH 8.6

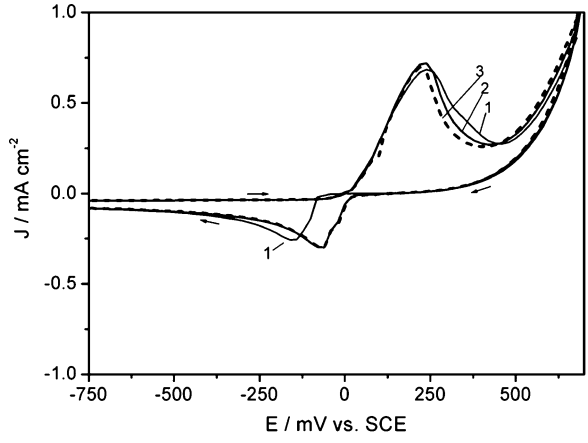

Fig. 6.7 A series of three consecutive cyclic voltammograms obtained for the vitreous carbon electrode in 20 mM Ag(I) + 0.25 M Na_2SO_3 + 0.1 M $NaNO_3$ bath, at a scan rate of 50 mV s^{-1}

concentration is shown. The change is linear with concentration emulating a diffusion limited relationship, which suggests that the main effect of sodium nitrate is upon the effective diffusion coefficient of the silver sulfite complex.

Three different substrate materials were tested for nanoparticles deposition: the glassy carbon electrode, titanium sheets, and ITO. The latter was chosen as a representative of a technical material of interest for its widespread use as industrial electrode substrate. Cycling voltammetry experiments from 0.7 to −0.7 V at a scan rate of 50 mV s^{-1} were performed in electrolyte of the following composition: Ag(I) 20 mM, Na_2SO_3 0.25 M, and $NaNO_3$ 0.1 M, at pH 8.6. A series of three successive voltammograms recorded in each condition is reported in Figs. 6.7 and 6.8 at the glassy carbon and titanium electrode, respectively. The behavior observed at the glassy carbon electrode conforms to the above presented results, with the further remark that after the first scan a remarkable shift towards more positive value of the nucleation potential is apparent. The voltammetric behavior observed at the titanium electrode does not show the standard features expected for a transient nucleation and growth process. In fact, during the first potential scan a steadily increasing cathodic current is observed, which is substantially

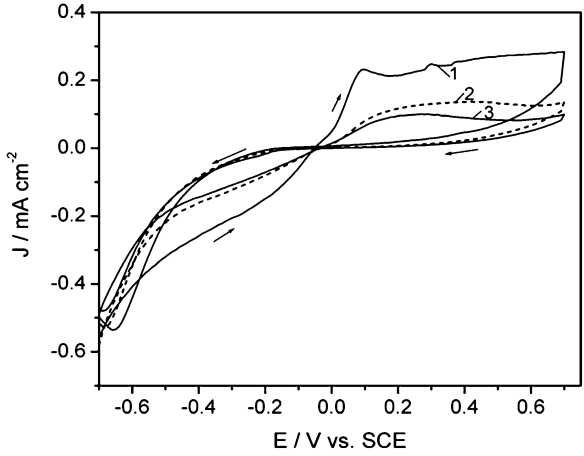

Fig. 6.8 A series of three consecutive cyclic voltammograms obtained at the titanium electrode in Ag(I) 20 mM, Na_2SO_3 0.25 M + $NaNO_3$ 0.1 M electrolyte at pH 8.6; scan rate 50 mV s^{-1}

reduced during the following cycling. In the anodic part of the reverse scan, the superposition of a current peak and a wave is observed during the first scan while upon cycling a single wave or a shallow broadened peak is consistently recorded. These features indicate that silver deposition on the titanium surface follows a quite different behavior compared to the glassy carbon electrode. Besides, the titanium surface shows evidence of inhibition upon cycling, as demonstrated by the current density decrease during both the cathodic and anodic part of the scan. The same type of study was performed with other concentration, obtaining similar results (Fig. 6.9).

Silver nanoparticles deposited on glassy carbon and titanium substrate are shown in Fig. 6.10. SEM images reported refer to relatively long pulse time duration, with one exception, to clearly visualize the deposition features. As expected, the glassy carbon surface performs much better compared to titanium sheets as long as the particle distribution is concerned. The glassy carbon electrode is inherently more fitted to a Volmer–Weber growth mode and in addition presents a highly polished surface allowing for a more uniform activity. The SEM image in Fig. 6.10 (top left) shows in fact that the surface is uniformly scattered with a dense array of particle of wide size

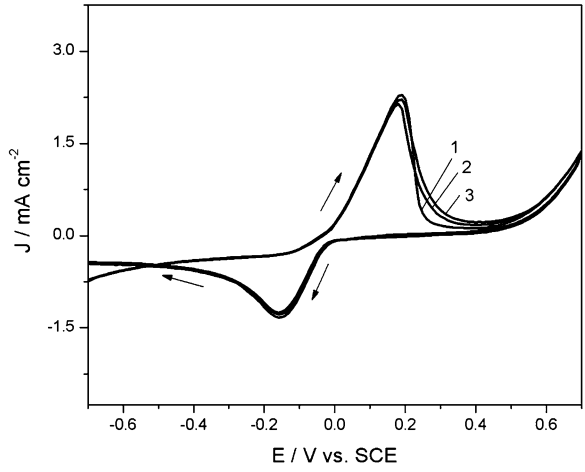

Fig. 6.9 A series of three consecutive cyclic voltammograms obtained at the ITO electrode in Ag(I) 20 mM, Na_2SO_3 0.25 M + $NaNO_3$ 0.1 M electrolyte at pH 8.6; scan rate 50 mV s^{-1}

distribution. Particle formation on titanium is characterized by the tendency to grow relatively large agglomerates as the potential pulse duration is increased, possibly also as a result of surface inhibition, as suggested by the above-presented voltammetric behavior.

This tendency towards clustering with deposition time is usually related to diffusion coupling between nearest-neighbor particles but, in the present case, it could also be triggered at the very stage of nucleation by the influence of the relatively high surface roughness of the substrate. Besides, it is worth noting that as the deposition time increases and particles agglomerates grow in size and number, the density of very fine particles, which are obtained at short pulse time, apparently lowers (Fig. 6.11).

The effect of the deposition potential is shown by the SEM micrographs presented in Fig. 6.12, also compared to image (b) in Fig. 6.10. Though not defined quantitatively, it is apparent that the increase of cathodic potential of a 50-ms pulse slightly reduces the tendency towards clustering and, as expected, increases the particle nucleation density.

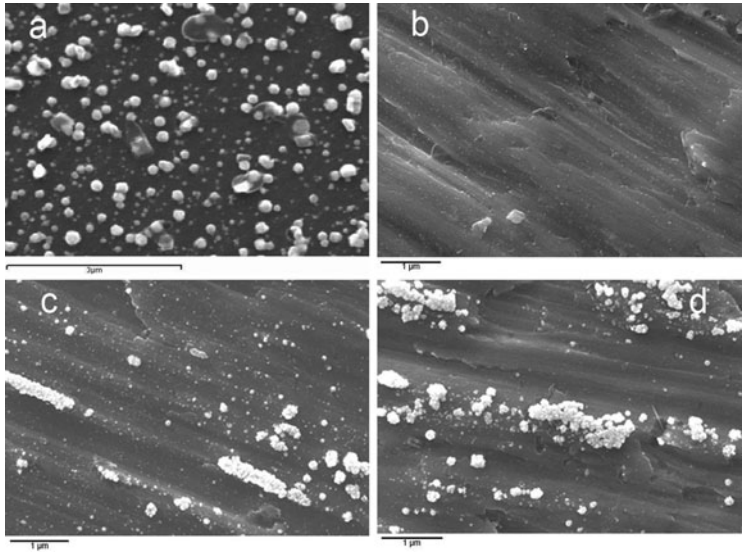

Fig. 6.10 Silver nanoparticles on glassy carbon electrode (**a**) (*top left*: −200 mV, 200 ms) and titanium substrate (*top right* and *bottom*: −200 mV); (**b**) 5 ms; (**c**) 50 ms; and (**d**) 100 ms from Ag(I) 20 mM, Na_2SO_3 0.25 M and $NaNO_3$ 0.1 M electrolyte at pH 8.6

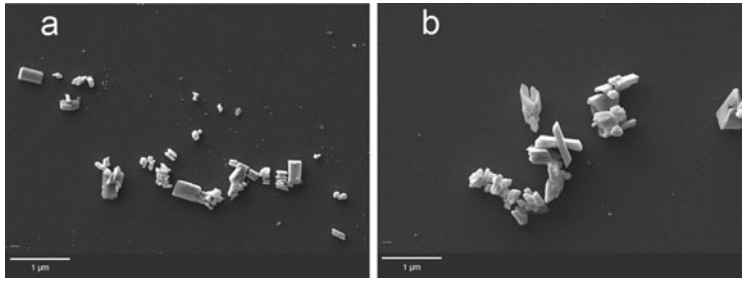

Fig. 6.11 Silver nanoparticles on ITO electrode: −200 mV; (**a**) 50 ms; (**b**) 100 ms from Ag(I) 20 mM, Na_2SO_3 0.25 M, and $NaNO_3$ 0.1 M electrolyte, at pH 8.6. The scale bar is 1 μm

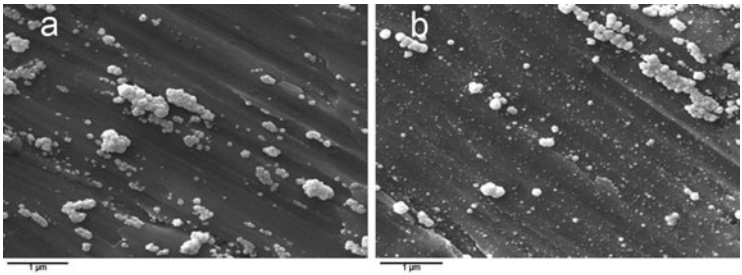

Fig. 6.12 Silver nanoparticles on titanium substrate from Ag(I) 20 mM, Na_2SO_3 0.25 M, and $NaNO_3$ 0.1 M electrolyte, at pH 8.6. Deposition potential: −400 (*left*), −600 mV (*right*). The scale bar is 1 μm

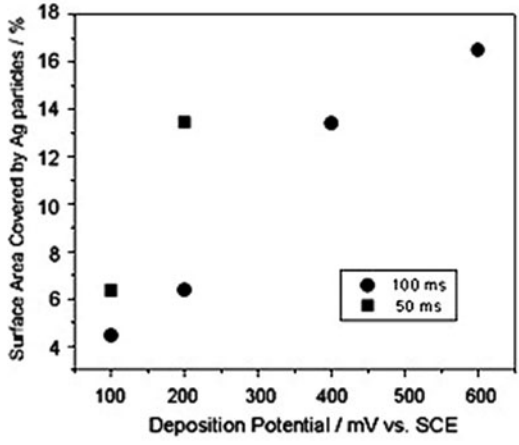

Fig. 6.13 Surface area of titanium electrode covered by silver particles versus the deposition potential for pulse duration of 50 and 100 ms. Electrolyte composition: Ag(I) 20 mM, Na_2SO_3 0.25 M, and $NaNO_3$ 0.1 M; pH 8.6

A pseudoquantitative assessment of the above-discussed effects of deposition potential and pulse duration on silver particles deposition on titanium can be made by evaluating the surface area covered by silver particles and aggregates as a function of these parameters. Some data are shown in the graph of Fig. 6.13 and they agree with the

above observations: with the increase of deposition time at given potential (in the time range considered in this work and relevant to the objective of particles formation) the coverage by silver particle is reduced; with the increase of cathodic potential at a given pulse duration, the surface area covered by silver particles increases.

6.6 Deposition of Gold Nanoparticles

Gold deposition from the $(NH_4)_3Au(SO_3)_2$ 10 mM, Na_2SO_3 0.1 M, and $C_2H_8N_2$ 10 mM, solution at pH 6.5, shows the characteristics of a highly irreversible process. In Fig. 6.14 cyclic voltammograms at the glassy carbon electrode at 50 mV s^{-1} scan rate are reported. From the first scan it may be inferred that the discharge of the Au(I) complex at the glassy carbon electrode is highly inhibited since no distinct feature, that could be related to gold deposition, is clearly seen but a shallow current wave starting from about −300 mV. This is soon superseded by a second current wave starting at about −500 mV.

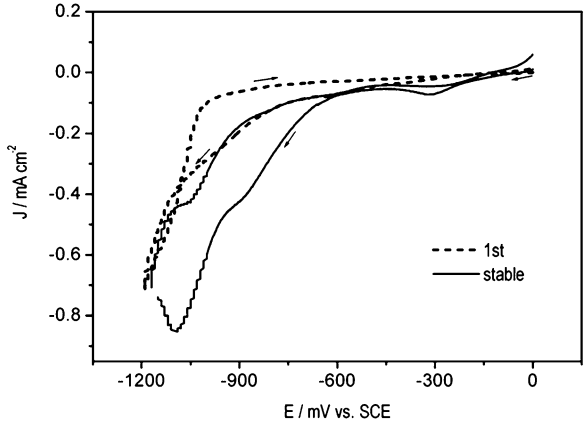

Fig. 6.14 Cyclic voltammograms at amorphous carbon electrode (first scan: *dashed line*; stable scan: *solid line*) in $(NH_4)_3Au(SO_3)_2$ 10 mM, Na_2SO_3 0.1 M, and ethylenediamine $C_2H_8N_2$ 10 mM, at pH 6.5; scan rate 50 mV s^{-1}, from 0 to −1.2 V

The latter can be attributed to the reduction of sulfite to dithionite ion, in agreement with early reports on the polarization behavior of Au(I) sulfite solution [64]. Upon cycling, a steady voltammogram is obtained where a distinct current peak for the discharge of the Au(I) sulfite complex appears at about −300 mV. This is followed by the reduction of sulfite to dithionite ion at the gold-plated surface at higher current density compared to the glassy carbon electrode. Similar features, though ill defined and poorly reproducible, could be recognized in voltammograms obtained by cycling at titanium electrode.

The voltammetric behavior of the gold deposition solution strongly suggests that particles formation may be controlled by a mechanism of progressive nucleation, as a result of kinetic control on the Au(I) sulfite complex discharge. However, the evidence from SEM observation of gold particles grown on titanium is not in line with this observation. SEM micrographs of gold particles deposited on titanium at changing pulse potential and 50 ms pulse duration are reported in Fig. 6.15. The nucleation density appears to be extremely sensitive to the deposition potential, possibly in connection with an inhibition effect of the side reaction of sulfite reduction. In fact, at −200 mV potential pulse, a uniform distribution of regularly sized gold particles is obtained, while at potential more negative than −400 mV a strong reduction in particles density is observed. However, notwithstanding the effect of deposition potential, SEM micrographs show that a highly uniform size distribution is obtained, even though the particle dimension is rather on the mesoscale (50–100 nm) than on the nanoscale dimension. Interestingly, quite different results were obtained when depositing gold particles on titanium sheets by potential sweeping from 0 to −1.2 V at changing scan rate. As shown by SEM micrographs reported in Fig. 6.16, particle size decreases and nucleation density increases as the potential scan rate is increased, but size distribution, as clearly shown by the insert in Fig. 6.16, is apparently worse than that obtained by a single potential pulse.

This behavior may be explained taking into account the influence of surface inhibition related to the electroreduction of sulfite, which could result in a twofold effect: inhibition of growth of already formed gold particles and nucleation of new particle on the titanium

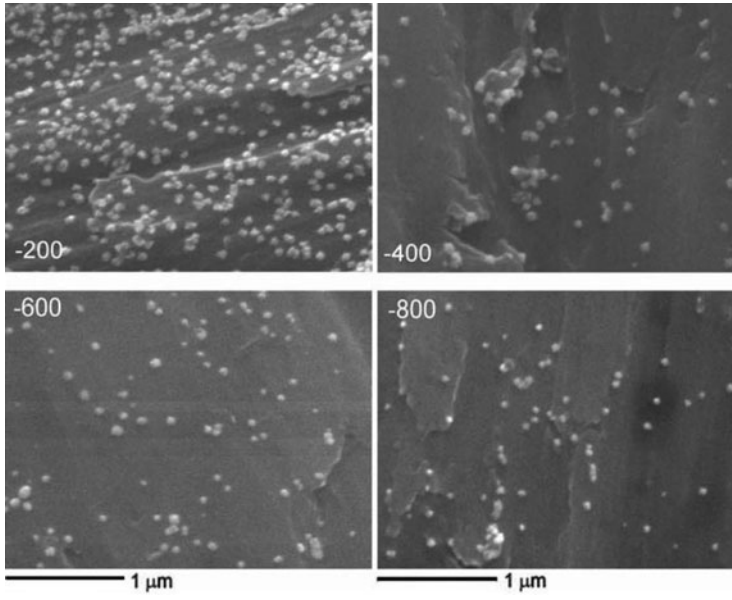

Fig. 6.15 SEM micrographs of gold particles on titanium deposited from $(NH_4)_3Au(SO_3)_2$ 10 mM, Na_2SO_3 0.1 M, and $C_2H_8N_2$ 10 mM, at pH 6.5, at changing potential, as indicated (vs. SCE) and 50 ms pulse duration. Scale bar is 1 μm

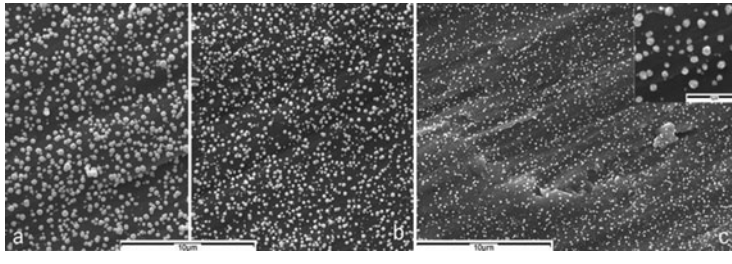

Fig. 6.16 SEM micrographs of Au particles on Ti deposited from Au(I) 10 mM, Na_2SO_3 0.1 M, and $C_2H_8N_2$ 10 mM solution, at pH 6.5, by potential sweeping from 0 to −1.2 at scan rate of 10 (**a**), 50 (**b**), and 200 mV s^{-1} (**c**). Scale bar is 10 μm; 1 μm in the *top-right* inset

surface as the deposition potential increases. Besides, it is also worth noting that particles size obtained by potential sweep is sensibly larger than that obtained by potential pulse deposition.

6.7 Galvanic Displacement of Nanoparticles on Silicon

The selective deposition of gold nanoclusters of controlled size on silicon surfaces by immersion plating in water-in-oil reversed micelle microemulsions is presented. Reversed micellar solutions are essentially dispersions of nanometer-sized water droplets in oil, stabilized by the presence of surfactant; they have long been used to synthesize metallic nanoclusters [65–67]. The conventional approach is based on the mixing and reacting of two different micellar solutions, e.g., one carrying a metal salt and the other carrying a reducing agent [68–70]. Nanocluster formation ensues upon micelle–micelle collision, material exchange between micelles, and subsequent reduction of the metal ions by the reducing agent. Here, a new strategy for directing nanocluster growth onto exposed silicon surfaces selectively has been adopted [71]. This selectivity is rooted in a galvanic displacement process. Galvanic displacement is a redox process, in which the substrate acts as the reducing agent for a species in solution. Thus, it achieves substrate selectivity, improved adhesion, and conformality, as demonstrated in recent thin film, interconnect, and MEMS applications. In these experiments, a water-based plating solution, containing hydrofluoric acid and a gold salt, is combined with sodium bis(2-ethylhexyl) sulfosuccinate (AOT, a surfactant) and heptane to produce a reversed micelle microemulsion. Metal cluster size is in good quantitative agreement with nominal micelle size over a wide range of values of the microemulsion parameter $R_{\text{micelle}}(\text{nm}) = 0.175R + 1.5$ (R = [water]/[AOT]). Figure 6.17a, b shows SEM images of gold and palladium nanoclusters on Si(100), respectively. A uniform coverage of the substrate is obtained [71].

The cluster-size distribution also appears fairly uniform; however, some larger aggregates can be observed and are attributed to cluster

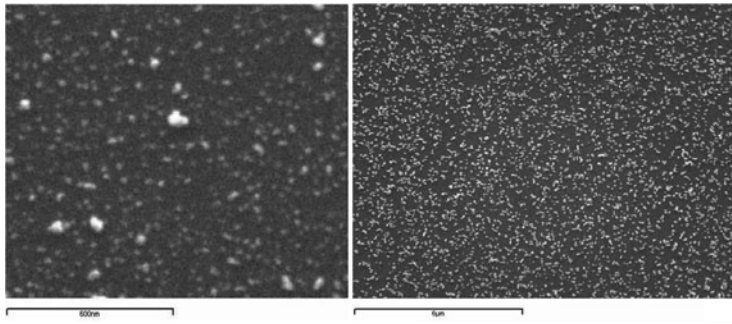

Fig. 6.17 SEM micrographs of gold (*left*) and palladium (*right*) clusters on silicon (*left*: $t = 15$ s, $R = 10$; *right*: $t = 600$ s, $R = 30$)

coalescence, especially for palladium. This phenomenon is well known from conventional studies of cluster formation in microemulsion systems, where cluster aggregates are in fact prevalent over single clusters. In the present case, it appears that cluster deposition by galvanic displacement from a single microemulsion is effective in reducing cluster aggregation.

6.8 Conclusions

Electrochemical synthesis of metal powder has been traditionally used for mass production of micrometer size powder being primarily used in powder metallurgy as well as other engineering applications. The electrochemical synthesis of metal nanoparticles and other nanostructures is being currently considered as a potential route for the development of advanced functional materials and devices in different technology area, including chemical sensing, magnetic storage, microelectronics, electroanalysis, and electrocatalysis. Nowadays, different nanomaterials are prepared by sonoelectrochemical methods. Silver and gold particles with size spanning from the nanoscale to the mesoscale were deposited from sulfite-based solutions. The proposed solution chemistry is reasonably stable and is shown to be a viable process for the electrochemical deposition of both Ag and Au particles. The

voltammetric behavior of the electrolytes is studied at different substrates surface, GC, Ti and ITO, showing that kinetic control plays a role in the discharge of the sulfite complex of Ag(I) or Au(I). Silver particles of size below 50 nm were easily obtained on glassy carbon substrate by potential-controlled deposition achieving a high nucleation density. On the other hand, size distribution was not easily controllable, most likely as a consequence of the irreversible nature of the discharge reaction of the Ag(I) complex. Silver particles deposition on titanium showed low nucleation density and a strong tendency to form large particles clusters and agglomerates, mostly in connection with surface irregularities. Gold particles were successfully deposited by either a potential pulse or a potential sweeping technique, achieving good results in terms of nucleation density. This was observed in particular when depositing on titanium substrate, on which by using a single potential pulse Au particles could be deposited with high nucleation density and uniform size distribution, though particle dimension was rather on the mesoscale than on the nanoscale dimension.

A novel method for depositing gold clusters on silicon surfaces, conformally and selectively, has been demonstrated. It is based on immersion plating in reversed micellar microemulsions of a plating solution containing metal and fluoride ions. A good correlation has been found between gold cluster size and micelle radius.

References

1. Chen CW, Takezako T, Yamamoto K, Serizawa T, Akashi M (2000) Colloids Surf A 169:107
2. Chen W, Cai WP, Liang CH, Zhang LD (2001) Mater Res Bull 36:335
3. Brust M, Walker M, Bethell D, Schiffrin DJ, Whyman R (1994) J Chem Soc Chem Commun 801
4. Magnusson M, Deppet K, Malm J-O, Bovin J-O, Samuelson L (1999) Nanostruct Mater 12:45
5. Collier PJ, Iggo JA, Whyman R (1999) J Mol Catal A Chem 146:149
6. Finot MO, Braybrook GD, McDermott MT (1999) J Electroanal Chem 466:234
7. Finot MO, McDermott MT (2000) J Electroanal Chem 488:125
8. Guerin S, Attard GS (2001) Electrochem Commun 3:544
9. Boccuzzi F, Chiorino A, Manzola M (2001) Mater Sci Eng C 15:215

10. Schimpf S, Lucas M, Mohr C, Rodemerck U, Bruckner A, Radnik J, Hofmeister H, Claus P (2002) Catal Today 72:63
11. El-Deab MS, Ohsaka T (2002) Electrochim Acta 47:4255
12. Popov KI, Pavlovic MG (1993) In: White RE, Conway BE, Bockris JO'M (eds) Modern aspects of electrochemistry, vol 24. Plenum, New York, p 299
13. Walter EC, Penner RM, Liu H, Ng KH, Zach MP, Favier F (2002) Surf Interface Anal 34:409
14. Sun M, Zangari G, Shamsuzzoha M, Metzger RM (2001) Appl Phys Lett 78:2964
15. Walter EC, Ng K, Zach MP, Penner RM, Favier F (2002) Microelectron Eng 61(62):555
16. Welch CM, Compton RG (2006) Anal Bioanal Chem 384:601
17. Arvia AJ, Salvarezza RC, Triaca WE (2004) J New Mater Electrochem Syst 7:133
18. Zoval V, Stiger RM, Biernacki P, Penner RM (1996) J Phys Chem 100:837
19. Zoval JV, Biernacki P, Penner RM (1996) Anal Chem 6:1585
20. Liu H, Penner RM (2000) J Phys Chem B 104:9131
21. Zoval JV, Lee J, Gorer S, Penner RM (1998) J Phys Chem B 102:1166
22. Anderson M, Gorer S, Penner RM (1997) J Phys Chem B 101:5895
23. Scheludko A, Todorova M (1952) Bull Acad Bulg Sci Phys 3:61
24. Ueda M, Dietz H, Anders A, Kneppe H, Meixner A, Plieth W (2002) Electrochem Acta 48:377
25. Reisse J, Francois H, Vandercammen J et al (1994) Electrochim Acta 39:37
26. Reisse J, Caulier T, Deckerkheer C et al (1996) Ultrason Sonochem 3:S147
27. Durant A, Delplancke JL, Libert V, Reisse J (1999) Eur J Org Chem 11:2845
28. Delplancke JL, Dille J et al (2000) Chem Mater 12:946
29. Zhu J, Liu S, Palchik O, Koltypin Yu, Gedanken A (2000) Langmuir 16:6396
30. Markov I, Boynov A, Toschev S (1973) Electrochim Acta 18:377
31. Gerisher H (1958) Z Electrochem 62:256
32. Price PB, Vermilyea DA (1958) J Chem Phys 28:720
33. Almawlawi D, Liu CZ, Moskovits M (1994) J Mater Res 9:1014
34. Liu KI, Chien CL, Searson PC, YuZhang K (1998) Appl Phys Lett 73:2222
35. Hulteen JC, Martin CR (1997) J Mater Chem 7:1075
36. Martin CR (1994) Science 266:1961
37. Strbac S, Maroun F, Magnussen OM, Behm RJ (2001) J Electroanal Chem 500:479
38. Strbac S, Magnussen OM, Behm R (1999) J Phys Rev Lett 83:3246
39. Moller FA, Magnussen OM, Behm R (1996) J Phys Rev Lett 77:5249
40. Kolb DM, Engelmann GE, Ziegler JC (2000) Solid State Ionics 131:69
41. Kolb DM, Engelmann GE, Ziegler JC (2000) Angew Chem Int Ed 39:1123
42. Ziegler JC, Engelmann GE, Kolb DM (1999) Z Phys Chem 208:151
43. Haruta M (1997) Catal Today 36:153
44. Maximov M et al (2000) Microelectron Eng 51:61
45. Yeager E, Hovorka F (1953) J Acoust Soc Am 25:443
46. Lickiss PD, McGrath VE (1996) Chem Br 32:47

47. Lighthill J (1978) Waves in fluids. Cambridge University Press, Cambridge, p 1221
48. Suslick KS (1990) Science 247:1439
49. Cornpton RG, Eklund JC, Marken F (1997) Electroanalysis 9:509
50. Moriguchi N (1934) J Chem Soc Jpn 55:749
51. Reisse J, Francois H, Vandercammen J, Fabre O, Kirsch-de Mesmaeker A, Maerschalk C, Delplancke JL (1994) Electrochim Acta 39:37
52. Durant A, Delplancke JL, Winand R, Reisse J (1995) Tetrahedron Lett 36:4257
53. Sáez V, Mason TJ (2009) Molecules 14:4284
54. Yeager E, Kovorka F, Dereska J (1957) J Acoust Soc Am 29:769
55. Saterlay AJ, Wilkins SJ, Goeting ChH, Foord JS, Compton RG, Marken F (2000) J Solid State Electrochem 4:383
56. Pollet B, Lorimer JP, Phull SS, Hihn JY (2000) Ultrason Sonochem 7:69
57. Goeting ChH, Foord JS, Marken F, Compton RG (1999) Diam Relat Mater 8:824
58. Han HM, Phillips GJ, Mikhalovsky SV, FitzGerald S, Lloyd AW (2008) J Mater Sci Mater Med 19:1787
59. Murali KR, Sasindran P (2004) J Mater Sci 39:6347
60. González-García J, Deseada Esclapez M, Bonete P, Vargas Hernández Y, Gaete Garretón L, Sáez V (2010) Ultrasonics 50:318
61. NIST Standard Reference Database 46, NIST Critically selected stability constants of metal complexes: Version 8.0
62. Hemmingsen T (1992) Electrochim Acta 37:2775
63. Bard AJ, Faulkner LR (1980) Electrochemical methods, fundamentals and applications. Wiley, New York
64. Derivaz J-P, Resin A, Losi S (1977) Surf Technol 5:369
65. Landfester K (2001) Adv Mater 13:765
66. Fletcher PDI, Howe AM, Robinson BH (1987) J Chem Soc Faraday Trans 83:985
67. Eastoe J, Fragneto G, Robinson BH, Towey TF, Heenan RK, Leng FJ (1992) J Chem Soc Faraday Trans 88:461
68. Arcoleo V, Cavallaro G, La Manna G, Turco Liveri V (1995) Thermochim Acta 254:111
69. Aliotta F, Arcoleo V, Buccoleri S, La Manna G, Turco Liveri V (1995) Thermochim Acta 265:15
70. Arcoleo V, Turco Liveri V (1996) Chem Phys Lett 258:223
71. Magagnin L, Bertani V, Cavallotti PL, Maboudian R, Carraro C (2002) Microelectron Eng 64:479